View metadata, citation and similar papers at core.ac.uk

brought to you by CORE

provided by Elsevier - Publisher Connector

Available online at www.sciencedirect.com

ScienceDirect

Progress in Natural Science: Materials International 24 (2014) 218–225

Progress in Natural Science Materials International

www.elsevier.com/locate/pnsmi
www.sciencedirect.com

Original Research

Optical parameters induced by phase transformation in RF magnetron sputtered TiO_2 nanostructured thin films

Prabitha B. Nair[a], V.B. Justinvictor[a], Georgi P. Daniel[a], K. Joy[a], K.C. James Raju[b], David Devraj Kumar[c], P.V. Thomas[a,*]

[a]Thin Film Lab, Post Graduate and Research Department of Physics, Mar Ivanios College, Thiruvananthapuram 695015, Kerala, India
[b]School of Physics, University of Hyderabad, Central University P. O., Hyderabad 500046, India
[c]College of Education, Florida Atlantic University, 3200 College Avenue Davie, FL 33314, USA

Received 30 January 2014; accepted 30 April 2014
Available online 2 June 2014

Abstract

Pure TiO_2 thin films were deposited onto quartz substrates using a ceramic TiO_2 target at an elevated substrate temperature of 573 K by RF magnetron sputtering, and an analysis of structural, optical and photoluminescence characteristics of the films upon phase transformation is reported in this paper. Structural investigations using X-ray diffraction revealed that the as-deposited film was amorphous in nature. Thermal annealing for 2 h at 873 K in air resulted in the formation of anatase phase, and a phase transformation to rutile was observed at 1073 K. An increase in grain size and an improvement in crystallinity were also observed on annealing. Rod- like rutile crystallites were observed in the SEM images of the film annealed at 1273 K. As-deposited films and films annealed up to 1073 K were highly transparent in the visible region with a transparency $>80\%$. Optical band gap of the films decreased upon thermal annealing which is attributed to phase transformation from amorphous to anatase and then to rutile. Optical parameters such as refractive index, optical conductivity and optical dielectric constant increased with increase in annealing temperature. Since rutile is the optically active phase, the superior refractive index of the film annealed at 1073 K along with its high transparency in visible region suggests the application of this film in antireflective coatings. Photoluminescence emission of maximum intensity was observed for the film annealed at 873 K, which exhibits anatase phase. Intense blue emission observed in this film makes it suitable for use in optoelectronic display devices.
© 2014 Chinese Materials Research Society. Production and hosting by Elsevier B.V. All rights reserved.

Keywords: RF magnetron sputtering; TiO_2 thin films; Dislocation density; Optical conductivity; Photoluminescence

1. Introduction

Nanocrystalline titanium dioxide (TiO_2) thin films have been investigated extensively in recent years because of their potential use as a low cost material in photovoltaics [1], gas sensors [2], photocatalysis [3], smart windows [4], antireflection coatings [5], optical filters [6] and as dye-sensitized solar cells [7,8]. Moreover, these films have good mechanical, thermal and anticorrosive properties required for practical uses. The atmospheric concentration of oxygen and UV light are all that is needed to drive oxidation of virtually any organic molecules adsorbed at the TiO_2 surface. Since such redox processes can occur at room temperature under solar or artificial UV light, a number of practical applications have been suggested including photoelectron chemical cells [1], antifog windows [9], and various self-cleaning devices [10].

TiO_2 can exist in amorphous form and also in three crystalline forms – anatase (A), rutile (R) and brookite (B). These phases are well distinguishable in terms of their physical properties. Anatase and rutile phases are tetragonal in nature

*Corresponding author. Tel.: +919447774782.
E-mail address: thomaspv_15@yahoo.com (P.V. Thomas).
Peer review under responsibility of Chinese Materials Research Society.

Production and hosting by Elsevier

http://dx.doi.org/10.1016/j.pnsc.2014.05.010
1002-0071/© 2014 Chinese Materials Research Society. Production and hosting by Elsevier B.V. All rights reserved.

while brookite exhibits an orthorhombic structure. Films in amorphous phase are widely used for optical coatings because of its optical anisotropy. Also due to its unique blood compatibility, amorphous titania films are promising candidates in the biomedical field. Optical band gap is higher for anatase compared to that of rutile (3.2 vs 3.0 eV). Anatase phase is known to exhibit better photocatalytic activity and is preferred over rutile for photodecomposition of environmental pollutants [11,12]. The rutile structure is very compact and thermodynamically most stable phase at all temperatures, and has higher refractive index than anatase (2.7 vs 2.52, at 550 nm wavelength). Rutile phase exhibits better optical activity than anatase and is used for antireflective and dielectric applications [13,14]. High dielectric constant of the material enables the use of TiO_2 thin films in micro-electronic devices [15]. The variation in properties, exhibited by amorphous, anatase and rutile thin films, have generated much interest in the study of their growth mechanisms. Since the optical properties of TiO_2 films also show interesting variations influenced by oxygen defects, impurities and crystalline size, the method of deposition and post-deposition thermal treatments are very important in inducing the desired properties in thin films.

In thin film form, TiO_2 is technologically important for use as light emitting devices and flat panel displays and hence the luminescence properties of the material have attracted much interest. Luminescence emission from TiO_2 nanopowders and nanowires has been reported in the literature [16,17]. The photoluminescence (PL) properties of rare-earth doped TiO_2 thin films have been reported by some authors [18–20]. Liu et al. [21] have reported PL emission in pure TiO_2 thin films on quartz substrates prepared by DC magnetron sputtering. They have concluded that post-deposition annealing can enhance PL properties of pure TiO_2 thin films. Huang et al. [22] have reported that incorporation of nitrogen in TiO_2 thin films deposited on Si(100) wafers enhances their visible PL significantly.

Structural control constitutes one of the major challenges in the design of suitable coating process for use in specific applications. In the present study, RF magnetron sputtering was used to deposit thin films. RF magnetron sputtering can produce highly uniform films having good adherence to the substrate. The method also offers the advantage of depositing films on a large area and on large scale which makes the method suitable for industrial applications [23]. Various parameters such as sputtering pressure, sputtering power, substrate temperature, and $Ar:O_2$ ratio can alter the structural and optical properties of thin films prepared by the sputtering method. The crystalline phases and microstructure are temperature dependent and hence post-deposition annealing has to be carefully carried out to enable the use of TiO_2 thin films for practical applications. This study aims to present a detailed analysis of the optical and photoluminescence properties of RF magnetron sputtered TiO_2 thin films, which have undergone structural changes due to post-deposition thermal annealing.

2. Experimental

The target used in the experiment was prepared by traditional ceramic process as described in our earlier paper [23]. The sputtering and post-deposition annealing conditions used in the study are given in Table 1. The as-deposited films are coded as T0 and the films annealed at 873, 973, 1073 and 1273 K are coded T873, T973, T1073, and T1273 respectively. All the films exhibited good adherence to the substrate. No cracking or peeling of the films was observed even after annealing at 1273 K.

Structural properties of the films were examined by standard X-ray diffraction (XRD) technique (Bruker AXS D8 Advance). Surface morphology was characterized by scanning electron microscopy (SEM) (Jeol Model JSM-6390LV) and atomic force microscopy (AFM) (SPA-400, SII, Inc. Japan – non contact mode). Optical transmission spectra were recorded in the wavelength range 300–900nm using a spectrophotometer (JASCO V- 550). Photoluminescence spectra was recorded in the wavelength range 350–600 nm using a spectroflurometer (Perkin-Elmer LS 55) employing a 40 W Xenon lamp as the excitation source. The samples were excited at 320 nm.

3. Results and discussions

3.1. Structural studies

Fig. 1 shows the XRD patterns of as-deposited and annealed TiO_2 thin films deposited at RF power 300 W and sputtering pressure 0.01 mbar. The as-deposited films were amorphous in nature, whereas the films annealed at 873 K showed the presence of anatase (101), (004) and (200) peaks at $2\theta = 25.35$, 37.86 and 48.19°, respectively. (101), (004), (200) and (105) peaks of the anatase at $2\theta = 25.28$, 37.93, 48.16 and 53.68° respectively, and a weak (110) peak of the rutile at $2\theta = 27.77°$ were observed in the film annealed at 973 K. Rutile (110), (101) and (211) peaks were observed at $2\theta = 27.45$, 36.07 and 54.48°, respectively, for the films annealed at 1073 K. For the film annealed at 1273 K, the diffraction peaks of (110), (111), (211) and (220) planes corresponding to rutile phase were observed at $2\theta = 27.93$, 41.89, 54.09 and 55.87°, respectively. During thermal annealing, the rearrangement of Ti and O atoms was such that the unit cell of TiO_2 tries to attain more stable and defect free configuration. Though anatase and rutile are tetragonal in nature, the value of c/a is closer to that of the most stable cubic lattice ($c/a = 1$) for rutile phase (0.65) than that for anatase ($c/a = 2.51$). Thus thermal annealing at higher temperatures ($>$ 1073 K) favors the complete phase transformation to rutile [13].

Table 1
Sputtering and post-deposition annealing conditions.

Sputtering gas	Argon
Sputtering pressure	0.01 mbar
RF power	300 W
Substrate temperature	573 K
Sputtering time	3 h
Substrate used	Quartz
Annealing temperature	873, 973, 1073, 1273 K
Annealing time	2 h
Annealing atmosphere	air

The average size of the crystallites (g) was determined using the Debye–Scherrer equation [24],

$$g = 0.9\,\lambda/\beta\,\cos\,\theta. \quad (1)$$

where, λ is the wavelength of the incident X-ray radiation (0.154 nm), β, the broadening of the diffraction line measured at half of its maximum intensity in radians, and θ, the Bragg's diffraction angle. Average crystallite size was found to increase with increase in annealing temperature, as shown in Table 2.

During the process of thin film growth, the coalescence of islands, dislocations was incorporated at the boundaries of two islands. Also, to relieve the strain at the film–substrate interface, dislocations may be set up in the crystal lattice. Dislocation density is the number of dislocation lines that intersect per unit area in the crystal. The particle size (g) is related to dislocation density (δ) in the film by the relation [25],

$$\delta = n/g^2. \quad (2)$$

where $n = 1$ for minimum dislocation density.

The lattice parameters were evaluated using Eq. [22],

$$1/d^2 = (h^2/a^2) + (k^2/b^2) + (l^2/c^2). \quad (3)$$

where d is the interplanar spacing, h, k, l represents the Miller indices of the planes and a, b and c, the lattice parameters. The obtained values of lattice parameters are given in Table 2. The values of lattice constants agree well with that of the bulk ($a_0 = 0.3785$ nm, $c_0 = 0.9513$ nm for anatase and $a_0 = 0.4593$ nm, $c_0 = 0.2959$ nm for rutile). The slight variation of lattice constants from that of the bulk value indicates a distortion in unit cell structure. The values of lattice distortion [23] are evaluated and are given in Table 2. This lattice distortion contributes to lattice strain. Strain relaxation was observed in the films annealed up to 1073 K, after which strain increases.

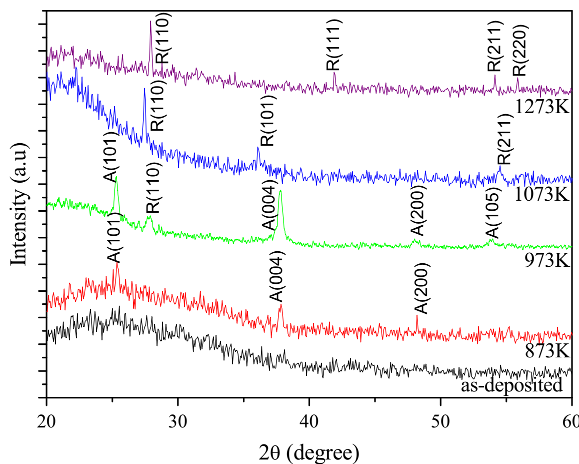

Fig. 1. XRD patterns of as-deposited and annealed TiO_2 thin films deposited at 0.01 mbar, 300 W, 573 K. [PDF 21-1276 (A), 21-1272(R)].

3.2. Surface studies

TiO_2 coatings have been analyzed by SEM and AFM techniques in order to study the surface structure, morphology and roughness. Annealing has strongly affected the surface features. The change in surface morphology with annealing temperature is mainly due to the differences in surface energy and surface migration properties, leading to the formation of surface structures and crystallites of varying sizes and nature. Fig. 2 shows the SEM micrograph of the samples T0, T873, T1073 and T1273. The as-deposited films exhibit a smooth surface. Surface scanning of the annealed films T873 and T1073 revealed a uniform base with the presence of some particulates of different sizes. Grain size was observed to increase for annealed films. This is due to coalescence of smaller grains effectively into larger grains with increasing temperature. On annealing at 1273 K, a rod-like surface morphology was observed. This can be attributed to the formation of tetragonal structure corresponding to the rutile phase, as was confirmed by XRD studies. Rod-like formation in pulsed laser deposited TiO_2 thin films, deposited at a higher oxygen pressure of 1 mbar and post annealed at 650 °C was reported by Shukla et al. [11].

Fig. 3 shows the surface morphologies of the samples T0 and T1073, observed by AFM. Agglomeration of particles as a result of thermal annealing was observed in the AFM image of the sample T1073 annealed at 1073 K. RMS roughness, which is the standard deviation of the surface from the mean plane within the sampling area [26], was found to increase from 2.10 to 3.36. This may be attributed to the grain growth on annealing [26]. The average grain size for the samples T0 and T1073 obtained from AFM images were 25.57 and 70.37 nm respectively.

Table 2
Structural parameters of as-deposited and annealed TiO_2 thin films deposited at 0.01 mbar, 300 W, 573 K.

Sample Phase	**T0** amorphous	**T873** anatase	**T973** mixed	**T1073** rutile	**T1273** rutile
Grain size (nm)	–	26.56	31.03	51.73	54.04
Lattice parameter (nm)					
a	–	0.3777	0.3789	0.4589	0.4511
c	–	0.9492	0.9475	0.2956	0.2906
Distortion		1.9329	0.3981	0.1234	−1.5735
Dislocation density($\times 10^{-3}$ nm^{-2})		1.4176	1.0386	0.3737	0.3423

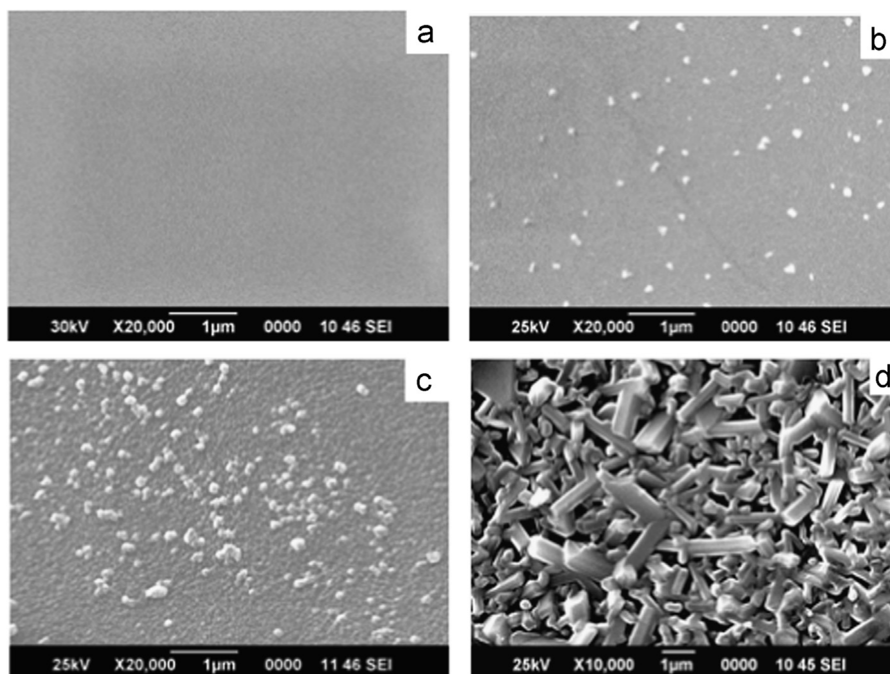

Fig. 2. SEM image of (a) as-deposited and annealed (b) 873 K (c) 1073 K (d) 1273 K TiO_2 thin films deposited at 0.01 mbar, 300 W, 573 K.

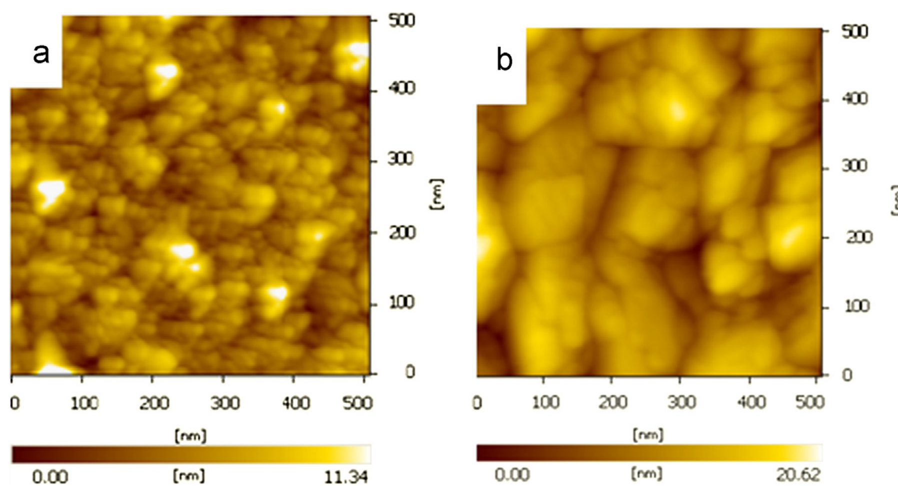

Fig. 3. AFM images of (a) as-deposited films and (b) films annealed at 1073 K deposited at 0.01 mbar, 300 W, 573 K.

3.3. Optical studies

Optical transmission spectra is one of the most widely used techniques for the analysis of band structure and optical band gap of both amorphous and crystalline materials. Fig. 4 shows the optical transmittance spectra of the as-deposited and annealed TiO_2 thin films. The films were highly transparent in the visible region with a transparency of $>80\%$. Slight fall in transmittance was observed on thermal annealing, which can be attributed to the increased surface roughness of the films observed from AFM patterns. But for the sample annealed at 1273 K (T1273), transparency falls sharply ($<10\%$), which is due to the microstructural and morphological changes in the film as a result of phase transformation, as seen in the SEM image.

The knowledge of optical constants of materials is of great significance in the design and analysis of optoelectronic devices. It is possible to determine optical constants, such as refractive index, absorption coefficient, and dielectric constant by analyzing transmittance spectrum. Optical constants and film thickness were evaluated using Swanepoel's envelope method [27], for the films annealed up to 1073 K. Since the optical transmission of coatings annealed at 1273 K is too weak in the visible region, the Swanepoel method does not allow the calculation of refractive index and other optical properties. The values of optical constants are given in Table 3. The as-deposited films have a thickness of 204 nm and a decrease in film thickness was observed on annealing. Refractive index was found to increase with increase in annealing temperature. This increase indicates densification of the films

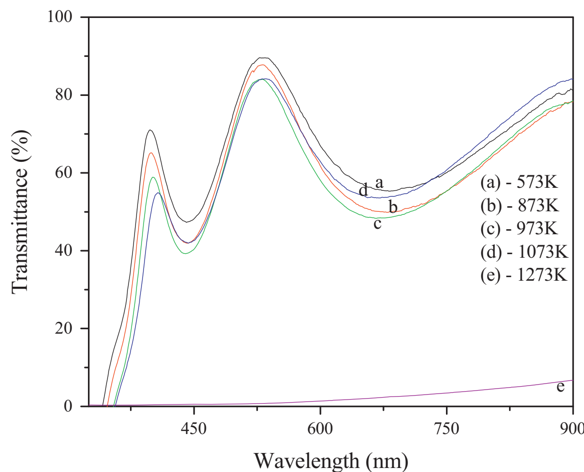

Fig. 4. Optical transmission spectra of as-deposited and annealed TiO_2 thin films deposited at 0.01 mbar, 300 W, 573 K.

Table 3
Optical parameters of as-deposited and annealed TiO_2 thin films deposited at 0.01 mbar, 300 W, 573 K.

Sample	T0	T873	T973	T1073
E_g (eV)				
direct	3.68	3.67	3.65	3.59
indirect	3.21	3.21	3.10	3.08
Thickness(nm)	204	195	193	193
At 550 nm,				
n	2.58	2.69	2.72	2.73
k	0.0639	0.0740	0.0743	0.0657
σ_{opt} ($s-^{-1}$)	7.72×10^{13}	8.58×10^{13}	1.08×10^{14}	1.37×10^{14}
ε_1	6.64	7.27	7.40	7.45
ε_2	0.3295	0.3992	0.4044	0.3587
tan δ	0.0495	0.0548	0.0546	0.0481

upon heat treatment and the formation of denser rutile phase [28,29]. Higher value of refractive index than that of the bulk indicates the nanocrystalline nature of the films. High transparency and highest value of refractive index (2.73) of the film annealed at 1073 K suggest the application of this film in antireflective coatings.

Absorption coefficient (α) is calculated as follows [30]:

$$\alpha=(1/t)\ln(1/T). \quad (4)$$

where t is the thickness of the film and T, the transmittance. Extinction coefficient (k) was evaluated using Eq. [30],

$$k=\alpha\lambda/4\pi. \quad (5)$$

A small increase in extinction coefficient was observed with increase in annealing temperature up to 973 K. This increase in extinction coefficient results in slight lowering of optical transmittance of the films. But for the film annealed at 1073 K, extinction coefficient showed a small decrease. This decrease in extinction coefficient is also reflected as a slight increase in transmittance of the sample T1073.

Above the threshold of fundamental absorption, optical transition is governed by the classical relation [30]:

$$\alpha h\nu=\alpha_o(h\nu-E_g)^m \quad (6)$$

where α_0 is a constant, a probability parameter for transition, E_g the optical band gap energy, $h\nu$ the photon energy and m, a constant which depends on the type of transition. It has been reported earlier that TiO_2 has three band gap transitions: for rutile and anatase the exact position of the transitions is slightly different, but there are two indirect transitions at approximately 3.0 and 3.2 eV, while there is a direct transition at 3.7 eV. These transitions are all in the UV region [31]. Direct and indirect band gaps in the range 3.58–3.79 eV and 3.05–3.4 eV, respectively depending on processing conditions is reported in the literature [32]. Serpone et al. [33] has established that both mechanisms can be observed in nanophase TiO_2.

The values of direct and indirect optical band gap are given in Table 3. Optical band gap was found to decrease with increase in annealing temperature. This decrease is consistent with the phase transformation from amorphous to anatase and then to rutile, occurring during the annealing process, which is evident in XRD patterns. Similar values of optical band gap were reported earlier by Hassan et al. for RF reactive magnetron sputtered TiO_2 thin films and by Habibi et al. for electron beam evaporated TiO_2 thin films [28,32]. It is well established that if dislocation density is high, it causes dilation in the spacing of atoms, which in turn influences the band gap of materials. An increased value for dislocation density suggests a higher band gap of the material [34]. The decrease in optical band gap on annealing is also consistent with the decrease in dislocation density given in Table 2.

TiO_2 has a dielectric constant (real part) of 6.3, at visible and near-infrared wavelengths, and the films are transparent at these wavelengths [35]. It was observed that both the real (ε_1) and imaginary (ε_2) part of dielectric constant increases with increasing photon energy and with annealing temperature (Table 2). The dissipation factor tan δ [36], was also found to increase with increasing photon energy and with annealing temperature. The variation of refractive index and dielectric constant (ε_1) with wavelength is shown in Figs. 5 and 6, respectively.

Absorption coefficient can be used to calculate the optical conductivity σ_{opt} [37]. An increase in optical conductivity was observed for the samples at high photon energies (Fig. 7). This may be due to the high absorbance of TiO_2 thin films and also due to the electrons excited by photon energy [38]. Optical conductivity also increases with annealing temperature.

3.4. Photoluminescence studies

Fig. 8 shows the room temperature PL spectra of the samples T0, T873 and T1073 excited at 320 nm. The PL emission in sample T1273 is very feeble with no remarkable spectral features, and hence is not shown in the figure. It is well established that the defects and vacancies in semiconductors and insulators can lead to the formation of localized states near the conduction band edge. Perturbations due to the defects

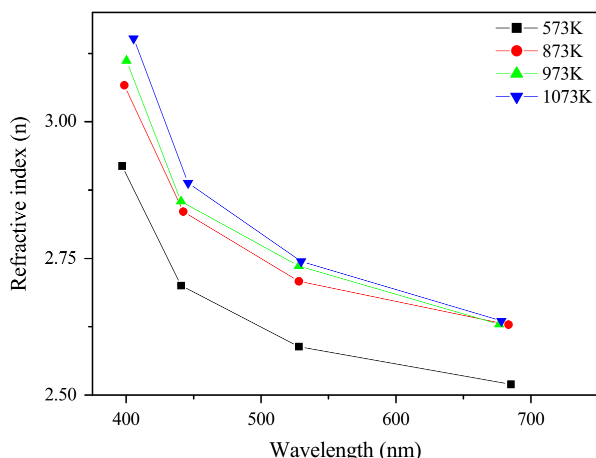

Fig. 5. Plot of refractive index versus wavelength for as-deposited and annealed TiO_2 thin films deposited at 0.01 mbar, 300 W, 573 K.

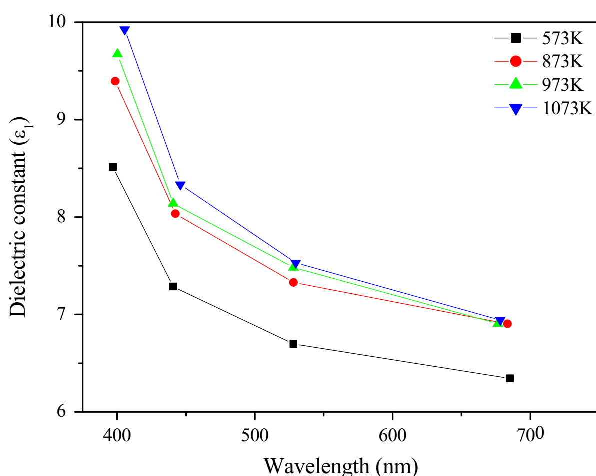

Fig. 6. Plot of real part of dielectric constant versus wavelength for as-deposited and annealed TiO_2 thin films deposited at 0.01 mbar, 300 W, 573 K.

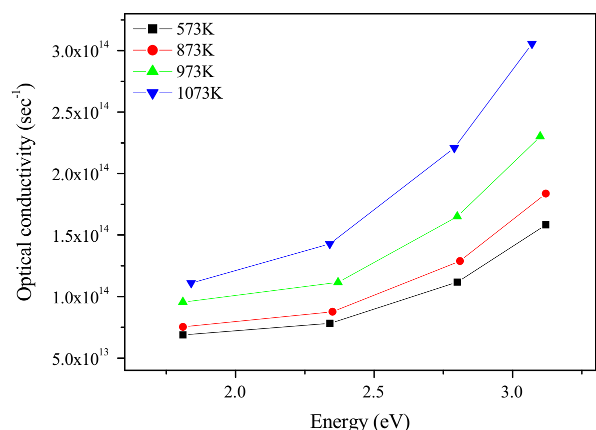

Fig. 7. Plot of optical conductivity versus photon energy for as-deposited and annealed TiO_2 thin films deposited at 0.01 mbar, 300 W, 573 K.

and impurities are characterized by discrete energy levels that lie within the band gap. When the concentration of such structural or compositional defects becomes sufficiently large,

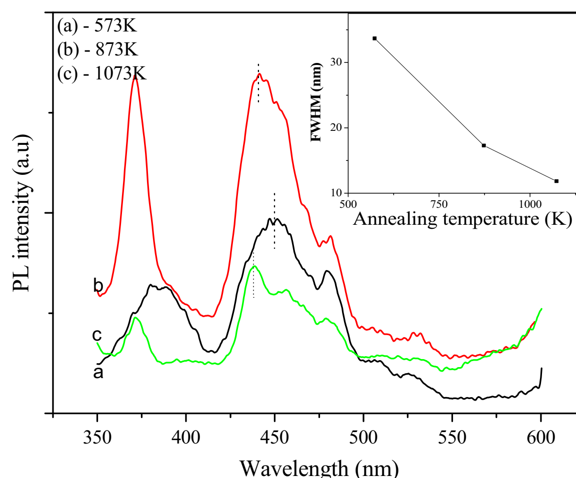

Fig. 8. Photoluminescence spectra of as-deposited and annealed TiO_2 thin films deposited at 0.01 mbar, 300 W, 573 K. Inset shows the variation of FWHM of the UV emission peak with annealing temperature.

they may either segregate to form cavities or distribute in the atom network. Intrinsic (delocalized) states may then be affected by the resulting distortion of the lattice. PL spectra for the samples are featured by emissions, both in the UV and visible regions. The UV emission originates from interband transition of electrons and the visible emission is due to transition of electrons from shallow donor level of the oxygen vacancies to the valence band. Oxygen vacancies occur in three different charge states: the neutral oxygen vacancy, the singly ionized oxygen vacancy and the doubly ionized oxygen vacancy, of which only the singly ionized oxygen vacancy can act as luminescent centers [39]. When the material is exposed to ultraviolet light, the oxygen vacancies which evolve during the growth of the material trap the holes generated by UV crystalline exposure. The recombination of hole with the electron already trapped at the oxygen vacancies emits light, which is generally in the visible region [13].

A broad UV emission peak was observed at 385 nm for the sample T0, and an intense UV emission at 371 nm was observed for the sample T873. Suisalu et al. [40] have attributed the UV emission peak at 3.36 eV (370 nm) to the excitons trapped at shallow level defects. Phase transition from amorphous to anatase phase has resulted in higher intensity of PL emission for the sample T873 [11]. But, intensity of UV emission peak at 371 nm decreases for the sample T1073. Usually, UV emission in thin films is related to its crystalline quality. Higher intensity of UV emission denotes better crystallinity of the film. According to XRD analysis, intensity of XRD peaks is higher for the sample T1073 than that for T0 and T873. This film also shows minimum value for lattice distortion (Table 2). Thus crystalline quality is better for the sample T1073 than that for T0 and T873. FWHM for the UV emission peak is minimum for the sample T1073 (inset of Fig. 8), which also indicates its better crystallinity. But intensity of PL emission is lowest for this sample. This decreasing trend of PL intensity with increase in annealing temperature was explained on the basis of various processes, such as, the recombination of the self trapped excitons, which is a combined

effect of the defect cores generated from oxygen vacancies and variation in particle size by Srivastava et al. [13].

PL emission of maximum intensity in the blue region was observed at 450, 441 and 438 nm for the samples T0, T873 and T1073 respectively. These peaks are due to the transition of electrons from the defect (trap) states to the valence band and are typical for nanostructured titania which is known to exhibit broad emission band in the range of 360–550 nm [13,21]. Intensity of blue emission is high for the sample T873, which was annealed at 873 K. It has been reported by Song et al. [41] that defects increase in the temperature range of 550–750 °C as TiO_2 nucleation occurs in this temperature range. When nucleation and crystallization occur, more electrons and holes excited from TiO_2 crystallites are trapped by these levels and hence radiative recombination increases. This accounts for the higher intensity of PL emission in the sample T873 annealed at 873 K. In addition, at lower temperatures the oxygen sub-lattice may contain many defects, both inside the film and at the surface [42]. Such defects produce various non-radiative cores and hence reduce light emission. The presence of such defect states has been reported in our earlier studies by analysis of the XPS spectra [23]. After annealing at high temperature, these non-radiative related defects could be reduced and restructured with a consequent increase in PL. However, the intensity of blue emission decreases for the sample T1073 annealed at 1073 K. Heat treatment at higher temperature promotes crystallite growth. No saturated ions decrease as crystallite size becomes larger. Also, the density of defects is reduced [41]. This leads to the decrease in PL intensity of the sample T1073. The dominant blue-shift of the visible emission in the blue region with annealing temperature, indicated by dotted lines in Fig. 8, along with considerable variation in PL intensity may be attributed to the effect of structural transformation from amorphous to anatase and then to rutile brought about by thermal annealing [13].

The oxygen impurities are a kind of intrinsic defects in TiO_2 lattice and form intermediate energy levels (trap levels) within TiO_2 band gap, introducing many recombination centers of photo-induced electrons and holes. The Ti–OH on TiO_2 surface is a kind of surface states, different from bulk defects because they can act as surface recombination centers [43]. The bulk impurities, mainly in the form of oxygen defects, act as active centers of indirect recombination. The weak shoulder emission peak at 480 nm (2.58 eV) for the samples T0, T873 and T1073 is associated with the indirect recombination via defects with the interaction of phonons in TiO_2 lattice [21].

The decrease in intensity of PL emission at higher annealing temperature (sample T1073) can be also attributed to thermal quenching. Excited luminescent centers are thermally activated through phonon interaction, which increases non radiative transition probability resulting in the decrease of emission intensity [44].

The PL emission bands in UV and visible region suggests the application of these films in various optoelectronic devices and as light emitters in the visible region. The change in luminescence intensity of the films with change in annealing temperature makes it suitable for optoelectronic temperature sensor applications. As RF magnetron sputtering can yield high quality, transparent and uniform films over a large area, these films find wide industrial application as visible light emitters. PL emission is highest for the sample T873, which establishes the fact that anatase films show better PL emission than the amorphous and rutile films. The increased PL activity of anatase phase has been reported in our earlier studies as well [23]. Hence these films in anatase phase can be made use of in the fabrication of optoelectronic display devices. This type of intense PL emission has not been so far reported for pure TiO_2 thin films, especially those prepared by RF magnetron sputtering.

4. Conclusions

Highly transparent TiO_2 thin films have been deposited on quartz substrates, using a ceramic TiO_2 target in argon atmosphere by RF magnetron sputtering. XRD studies reveal phase transformation from amorphous to anatase and then to rutile with increase in annealing temperature. RF magnetron sputtering at 300 W, 0.01 mbar sputtering pressure, at substrate temperature 573 K for 3 h, and subsequent thermal annealing in air for 2 h at 873 K is the optimized condition for producing anatase films, which are metastable in nature. The calculated values of lattice constants slightly varied from that of bulk values, indicating distortion in unit cell structure. SEM and AFM analyses show that thermal annealing strongly affects the surface morphology of the samples. For the films annealed at 1273 K, where rutile phase exhibited, rod-like surface morphology was observed in SEM images. An increase in RMS roughness was observed on annealing, which is attributed to grain growth. A decrease in optical band gap was observed with increase in annealing temperature. This change is consistent with the phase transformation from amorphous to anatase and then to rutile observed in XRD analysis. The decrease in dislocation density on thermal annealing also contributes to the decrease in band gap. The increase in refractive index on annealing is attributed to the film densification. Extinction coefficient, optical conductivity and optical dielectric constant showed an increase with annealing temperature. The high refractive index of the optically active rutile phase is of special interest in the design of antireflective coatings. Intense PL emission in the UV and visible region was observed for the films annealed at 873 K. These films in anatase phase have potential applications in optoelectronic devices and in display devices.

Acknowledgment

One of the authors (P.V.T) wishes to thank the University Grants Commission, New Delhi for the financial assistance (F.no.39-503/2010(SR)).

References

[1] M Gratzel, Nature 414 (2001) 338–344.
[2] W Gopel, G Reinhardt, in: H Baltes, J Hesse (Eds.), Sensors, Wiley, Weinheim, 1996, pp. 47–57.
[3] H Gnaser, B Huber, Ch. Ziegler, in: H.S Nalwa (Ed.), Encyclopedia of Nanoscience and Nanotechnology, American Scientific Publishers, Stevenson Ranch, 2004, pp. 505–535.

[4] H. Dislich, P. Hinz., J. Non-Cryst. Solids 48 (1982) 11–16.
[5] B. Yoldas, Appl. Opt. 19 (1980) 1425–1429.
[6] R.W. Phillips, J.W. Dodds, Appl. Opt. 20 (1981) 40–47.
[7] Y.C. Shih, A.K Chu, W.Y. Huang, J. Nanosci. Nanotechnol. 12 (2012) 3070–3076.
[8] S.Y. An, J.H Park, J.H Kim, C.J. Choi, H Kim, K.S. Ahn, J. Nanosci. Nanotechnol. 12 (2012) 3398–3409.
[9] R. Wang, K. Hashimoto, A. Fujishima, M. Chikuni, E. Kojima, A. Kitamura, M. Shimohigoshi, T. Watanabe, Nature 338 (1997) 431–432.
[10] O. Lergini, E. Oliveros, A.M. Braun, Chem. Rev. 93 (1993) 671–698.
[11] G. Shukla, P.K. Mishra, A. Khare, J. of Alloys Compd. 489 (2010) 246–251.
[12] H. Ogawa, T. Higuchi, A. Nakamura, S. Tokita, D. Miyazaki, T. Hattori, T. Tsukamoto, J. Alloys Compd. 449 (2008) 375–378.
[13] A.K. Srivastava, M. Deepa, S. Bhandari, H. Fuess, Nanoscale Res. Lett. 4 (2009) 54–62.
[14] I. Hotovy, A. Pullmannova, M. Predanocy, J. Hotovy, V. Rehacek, T. Kups, L. Spiess, J. Electr. Eng. 60 (6) (2009) 354–357.
[15] W.D. Brown, W.W. Grannemann, Solid State Electron. 21 (1978) 837–846.
[16] J.D. Fidelus, M. Barczak, K. Michalak, Z. Fekner, A. Duzynska, A. Jusza, R. Piramidowicz, C.J. Monty, A. Suchocki, J. Nanosci. Nanotechnol. 12 (2012) 3760–3765.
[17] P. Chinnamuthu, A. Mondal, N.K. Singh, J.C. Dhar, S.K. Das, K.K. Chattopadhyay, J. Nanosci. Nanotechnol. 12 (2012) 6445–6453.
[18] R.P. Merino, A.C. Gallardo, M.G. Rocha, I.H. Calderon, V. Castano, R. Rodriguez, Thin Solid Films 401 (2001) 118–123.
[19] A.C. Gallardo, M.G. Rocha, R.P. Merino, M.P.V. Quesada, I. H. Calderon, Appl. Surf. Sci 212-213 (2003) 583–588.
[20] C. Jia, E. Xie, A. Peng, R. Jiang, F. Ye, H. Lin, T. Xu, Thin Solid Films 496 (2006) 555–559.
[21] B. Liu, X. Zhao, Q. Zhao, X. He, J. Feng, J. Elect. Spect. Rel. Phenom. 148 (2005) 158–163.
[22] A.P. Huang, Z.F. Di, P.K. Chu, Surf. Coat.Technol. 201 (2007) 4897–4900.
[23] P.B. Nair, V.B. Justinvictor, G.P. Daniel, K. Joy, V. Ramakrishnan, P. V. Thomas, Appl. Surf. Sci. 257 (2011) 10869–10875.
[24] L.V. Azaroff, in: Elements of X-ray Crystallography, McGraw Hill, Newyork, 1968.
[25] S.S. Cetin, S. Corekci, M. Cakmak, S. Ozcelik, Cryst. Res. Technol. 46 (11) (2011) 1207–1214.
[26] G.P. Daniel, V.B. Justinvictor, P.B. Nair., K. Joy, P. Koshy, P.V. Thomas, Physica B 405 (2010) 1782–1786.
[27] R. Swanepoel, J. Phys. E: Sci. Instrum. 16 (1983) 1214–1222.
[28] M.M. Hassan, A.S.M.A. Haseeb, R. Saidur, H.H. Masjuki, M. Hamdi, Opt. Mater. 32 (6) (2010) 690–695.
[29] G. Hass, Vacuum 2 (1952) 331–345.
[30] J. Tauc, Mater. Res. Bull. 5 (8) (1970) 721–729.
[31] Y. Liu, J.I. Dadap, D. Zimdars, K.B. Eisenthal, J. Phys. Chem. B 103 (1999) 2480–2486.
[32] M.H. Habibi, N. talebian, J.H. Choi, Dyes Pigment. 73 (2007) 103–110.
[33] N. Serpone, D. Lawless, R. Khairutdinov, J. Phys. Chem. 99 (1995) 16646–16654.
[34] M. Pandiaraman, N. Soundararajan, C. Vijayan, J. Ovonic Res. 7 (1) (2011) 21–27.
[35] H. Kakiuchida, P. jin, M. Tazawa, Thin Solid Films 516 (2008) 4563–4567.
[36] M.M.A. Aziz, I.S. Yahia, L.A. Wahab, M. Fadel, M.a. Afifi, Appl. Surf. Sci 252 (2006) 8163–8170.
[37] J.I. Pankove, in: Optical Processes in Semiconductors, Dover Publications Inc., Newyork, 1975, p. 91–107.
[38] F. Yakuphanoglu, A. Cukurovali, I. Yilmaz, Opt. Mater. 27 (2005) 1366–1368.
[39] J. Lim, K. Shin, H.W. Kim, C. Lee, Mater. Sci. Eng. B 107 (2004) 301–304.
[40] A. Suisalu, J. Aarik, H. Maendar, . Sildos, Thin Solid Films 336 (1998) 295–298.
[41] C.F. Song, M.K. Lu, P. Yang, D. Xu, D.R. Yuan, Thin Solid Films 413 (2002) 155–159.
[42] K. Joy, I.J. Berlin, P.B. Nair, J.S. Lakshmi, G.P. Daniel, P.V. Thomas, J. Phys. Chem. Solids 72 (2011) 673–677.
[43] B. Liu, L. Wen, X. Zhao, Mater. Chem. Phys. 106 (2007) 350–353.
[44] J.S. Kim, Y.H. Park, S.M. Kim, J.C. Choi, H.L. Park, Solid State Commun. 133 (2005) 445–448.